Investigation of Optimal Split Ratio of 6-Slot/2-pole High Speed Permanent Magnet Motor with Toroidal Winding

F. Xu, T. R. He, Z. Q. Zhu, *Fellow, IEEE*, H. Bin, D. Wu, L. M. Gong, and J. T. Chen

***Abstract*—Split ratio, i.e. the ratio of stator inner diameter to outer diameter, has a closed relationship with electromagnetic performance of permanent magnet (PM) motors. In this paper, the toroidal windings with short end-winding axial length are employed in the 6-slot/2-pole (6s/2p) PM motor for high speed applications. The split ratio is optimized together with the ratio of inner slot to outer slot area, i.e. slot ratio, considering stator total loss (stator iron loss and copper loss). In addition, the influence of maximum stator iron flux density and tooth-tip on the optimal split ratio, slot ratio, and average torque is investigated. The analytical predictions show that when the slot ratio is 0.5, the maximum torque can be achieved, and the optimal split ratio increases with the decrease of slot ratio, as confirmed by the finite element (FE) analyses. Finally, some of predicted results are verified by the measured results of 6s/2p prototype motor with 0.5 slot ratio.**

***Index Terms*—High speed, Optimal split ratio, Permanent magnet motor, Slot ratio, Toroidal winding.**

I. Introduction

High speed permanent magnet (HSPM) motors have advantages of high power density and high efficiency. They are widely employed in many industrial applications, such as electric turbochargers, automotive superchargers, micro gas turbines, compressors, blowers, pumps, hybrid electric vehicles, turbo-molecular pumps, and machine tool spindle drives [1]-[8]. For domestic appliances, e.g. vacuum cleaners, small size low power HSPM motors offer advantages in high power density and high efficiency which is desirable and attractive [9]. There are different slot/pole combinations has been employed in this area, such as 3-slot/2-pole (3s/2p) motor with non-overlapping windings [9][10], 6-slot/2-pole (6s/2p) motors with non-overlapping/overlapping windings [3],[11]-[12].

Manuscript received August 07, 2022; revised October 21, 2022; accepted November 30, 2022. date of publication December 25, 2022; date of current version December 18, 2022.

F. Xu, T. R. He, and Z. Q. Zhu are with the University of Sheffield, Department of Electronic and Electrical Engineering, Mappin Street, Sheffield, S1 3JD, UK (e-mail: fxu7@sheffield.ac.uk; hetianran@tongji.edu.cn; z.q.zhu@sheffield.ac.uk)

H. Bin, D. Wu, L. M. Gong, and J. T. Chen are with Motors and Drives Center, Midea Group Corporate Research Center, Shanghai, 200131, China (email: hong.bin@midea.com; wudi9@welling.com.cn; gongliming@midea.com; chenjintao@welling.com.cn)

(Corresponding author: Z. Q. Zhu)

Digital Object Identifier 10.30941/CESTEMS.2022.00045

In literature, [10] designs a 3s/2p HSPM motor for hand piece tool. The rotor with a solid PM together with stainless steel shaft is designed to improve the mechanical strength for high speed operation (150 krpm). In [9], a 20 krpm 3s/2p HSPM motor is designed for friction welding unit. It shows that compared with conventional motor, HSPM motor with high frequency result in large stator iron loss, which cannot be neglected in the optimization. 3s/2p PM motors with inherent unbalanced magnetic force (UMF) may lead to vibration and noise, and thus, a 6s/2p PM motor with no UMF is more attractive for high speed applications. In [11], a 6s/2p HSPM motor with tooth-coil windings is designed and analyzed. The Inconel material (Inconel-718) for magnet protection covers the rotor surface and the magnets are magnetized radially. The differences between 3s/2p and 6s/2p HSPM motors with tooth-coil windings are compared in [12]. The results show that since the 3-slot motor has richer spatial harmonics caused by slotting effect, the 6-slot motor has less rotor eddy current loss, which is desirable for high speed application. However, the 6s/2p HSPM motor with non-overlapping windings has relatively low winding factor (0.5). Therefore, a 6s/2p HSPM with two slot-pitch windings is proposed to increase the output torque and torque density since it has large winding factor (0.866) and relatively short axial length [14].

As another kind of non-overlapping windings, toroidal windings with short end-winding axial length can be beneficial for better rotor mechanical stiffness under high speed rotation, which have been employed for several applications, such as micro turbine, gas turbine, and air compressor [15]-[17]. [15] and [16] design 6s/2p HSPM generators for micro turbines and for mesoscale gas turbines, respectively. In [17], three 6s/2p HSPM motors with different rated speeds (150 W at 200 krpm, 42 W at 90 krpm, 3.7 kW at 240 krpm) are designed. It is found that the high external leakage of the armature field of toroidal windings will lead to eddy current losses in the housing, which may account for 50% of total motor loss and should be considered. [18] investigates the effect of slot number on the electromagnetic performances of 2-pole HSPM motors with toroidal windings, accounting for back electromotive forces (back-EMF), cogging torque, electromagnetic torque, different loss components including losses in the housing, winding inductance, and UMF. Overall, toroidal windings have advantages of short end-winding axial length, simple structure, easy manufacturing process, and modular design.

In general, the stator outer diameter is fixed, the design of stator inner diameter, i.e. split ratio (SR), has a great effect on motor torque, power capability and overall manufacturing cost [10],[19],[20]. In literature, the optimal SR has been investigated under different design considerations and restrictions [8] [21]-[25]. For low- and moderate-speed PM motors with overlapping and non-overlapping windings, the optimal SR has been investigated comprehensively in [22]. Moreover, the influences of operation mode, air-gap flux density distributions, tooth-tips and end-windings on optimal SR are discussed. For HSPM motors, [8] analyses the optimal SR and optimal flux density ratio by analytical method. Considering the stator iron loss, [21] optimizes the SR for the highest efficiency. [23] considers the stator iron loss and mechanical constraints for optimal SR in 6-slot/4-pole HSPM motor. [24] derives an analytical expression of the optimal SR accounting for both stator and rotor loss limitations in small size HSPM motors. For HSPM motors with toroidal windings, [18] uses finite element (FE) method to optimize the SR for maximum torque with fixed current density and stator thermal limitation.

It is worth noting that in existing research, the outer and inner slot areas are all defined as the same value for maximum electrical load. However, in order to improve the heat dissipation capability of HSPM motor, the partial areas in outer slots of motors with toroidal windings can be used as the cooling channels under forced-air cooling and the slot ratio, i.e. the ratio of inner slot area to total slot area, will be changed accordingly. Therefore, in this paper, the influence of slot ratio on the optimal SR of the 6s/2p HSPM motor with toroidal windings (TWHSPM) will be investigated, which is a main innovation of this research. In addition, the effect of stator total loss and the maximum stator iron flux density will be considered.

In section II, the motor topology including end-winding model are described. The optimal SR for maximum torque with fixed stator total loss is investigated analytically in section III. The influence of different design parameters on the optimal SR, including slot ratio, maximum stator iron flux density, and tooth-tips are illustrated in Section IV. A porotype motor is manufactured and tested in section V. Section VI is the conclusion.

II. Motor Topology

The cross section of a 6s/2p TWHSPM motor is shown in Fig. 1. The slot is divided into inner and outer slots by stator yoke due to toroidal winding configuration. The toroidal windings mean the winding is wound on the stator yoke, one side of the coil is located in the outer slot and the other side is located in the inner slot. It is worth noting that the connection polarities of the coils A1 and A2 for the same phase in the inner slot are opposite, Fig. 1. Under high speed operation, a 2-pole ring magnet with parallel magnetization is adopted to reduce the operating frequency, which is protected by a stainless steel sleeve, and a magnetic shaft is adopted to improve output torque. In addition, the straight tooth without tooth-tips is employed for simplifying manufacture process. Table I shows the basic parameters of the motor.

For the motor with toroidal windings, only conductors in the inner slot of winding can link the flux and produce the back-EMF, the rest conductors, i.e. the conductors in the outer slot only form the current circuit loop. Therefore, the winding factor (k_w) of the 6s/2p combination is 0.5 as the winding in the outer slot can be treated as a part of end-winding [18]. Fig. 2 shows the end-winding model includes two end parts linking the outside and inside conductors which are assumed to be semi-circular. The total end-winding length (l_e) of one coil can be calculated as

$$l_e = 2l_{er} + l_a = 2\left[\frac{\pi}{2}\left(\frac{h_{out}+h_{in}}{2}+h_y\right)+2l_{ex}\right]+l_a \quad (1)$$

where h_{out}, h_{in} and h_y depict outer tooth height, inner tooth heights, and stator yoke height, respectively. l_{er} and l_a are the radial end-winding length and the stator active length, respectively. In addition, based on the manufactory process the extra part of end-winding length (l_{ex}) is variable and considered in this paper.

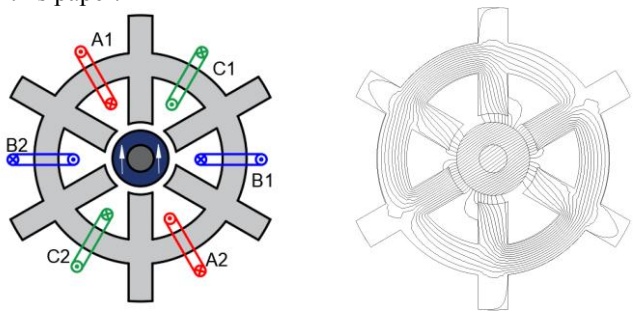

(a) (b)

Fig. 1. Cross section and flux distribution of the 6s/2p TWHSPM motor. (a) Cross section. (b) Flux distribution.

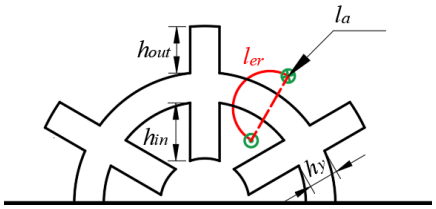

(a)

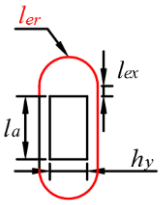

(b)

Fig. 2. End-winding model of the motor with toroidal windings. (a) Model 1. (b) Model 2.

TABLE I
BASIC PARAMETERS OF TWHSPM MOTOR

Rated speed (krpm)	110	Shaft diameter (mm)	5
Stator outer radius (mm)	27	Remanence (T)	1.3
Stator active length (mm)	9.1	Magnetization	Parallel
Air-gap length (mm)	1.55	Number of series turns	37

III. Optimal Design for Maximum Torque

In this section, the SR of the 6s/2p TWHSPM motor is optimized for maximum average torque by analytical method. It is assumed that the inner slot area equals to outer slot area, and the outer tooth and inner tooth have the same width although the outer teeth are only used for mechanical supporting. In HSPM motors, high frequency will result in large stator iron loss. Therefore, the optimal SR of the HSPM motor takes both stator iron loss and copper loss into account. The stator iron loss is calculated by the Bertotti module [26]

$$P_{fe} = m_{fe} W_{fe} \tag{2}$$

$$W_{fe} = k_{hy} f B_{fe} + k_{ex} f^{1.5} B_{fe}^{1.5} + k_{ec} f^2 B_{fe}^2 \tag{3}$$

where W_{fe} represents the iron loss density, k_{hy}, k_{ex}, and k_{ec} depict the hysteresis coefficient, the eddy current coefficient, and the excess loss coefficient, respectively. f is the fundamental frequency. B_{fe} depict the maximum stator iron flux density. m_{fe} is the stator mass, which can be calculated by

$$\begin{aligned} m_{fe} &= \rho_{fe} A_{fe} l_a \\ &= \rho_{fe} l_a \left\{ \frac{\left[\left(D_s - h_{out} \right)^2 - \left(D_s - h_{out} - D_i \right)^2 \right] \pi}{4} - A_{sin} \right\} \end{aligned} \tag{4}$$

where p_{fe} and D_i depict the iron mass density and the stator inner diameter, A_{sin} is the inner slot area, A_{fe} is the stator iron area without the area of outer slot teeth since there are no flux in outer slot teeth and their iron flux densities are equal to almost zero.

In order to limit the motor operating temperature, the optimization employs a fixed stator loss, which counting for stator iron loss and copper loss. In this case, under forced-air cooling, the stator thermal limitation can be derived as [1] [27]

$$P_{limit} = h v_m \pi D_s l_a \tag{5}$$

where D_s is the stator outer diameter, and h is the overall heat transfer coefficient of 100 W/(°Cm^2). Accounting for 'E' insulation class, the winding hotspot temperature must be lower than the maximum allowed temperature v_m of 120℃ for slotted structure. As mentioned in section II, the coils are wounded toroidally and thus, the length of end-winding is non-negligible. In general, HSPM motors are designed under 120° electrical brushless DC operation mode. Therefore, the copper loss is given by

$$P_{cu} = 2 I_a^2 \rho_{cu} \frac{(l_a + l_e) N_s}{A_{cond}} \tag{6}$$

where I_a, ρ_{cu}, N_s and A_{cond} depict the amplitude of phase current, the resistivity of copper, the number of series turns per phase, and the cross-section area of conductors, respectively. Since the copper loss equals to (P_{limit} - P_{fe}), the amplitude of phase current is given by

$$I_a = \sqrt{\frac{\left(P_{limit} - P_{fe} \right) A_{cond}}{2 \rho_{cu} (l_a + l_e) N_s}} \tag{7}$$

and the electromagnetic torque (T_{em})is obtained as

$$\begin{aligned} T_{em} &= 2 D_s l_a N_s k_w B_g I_a \\ &= 2 B_g (D_i - l_g) l_a N_s k_w \sqrt{\frac{(P_{limit} - P_{fe}) A_{cond}}{2 \rho_{cu} (l_a + l_e) N_s}} \end{aligned} \tag{8}$$

where l_g and B_g depict the air-gap length and the maximum air-gap flux density. B_g can be calculated by [8]

$$B_g = \frac{B_r \left[1 - \frac{R_r^2}{R_m^2} \right] \left[\frac{R_m^2}{R_i^2} - \frac{R_m^2}{\left(R_i - l_g/2 \right)^2} \right]}{\left[1 + \frac{R_m^2}{R_i^2} \right] \left[1 - \frac{R_r^2}{R_m^2} \right] + \mu_r \left[1 - \frac{R_m^2}{R_i^2} \right] \left[1 + \frac{R_r^2}{R_m^2} \right]} \tag{9}$$

where B_r and μ_r are the remanence and relative recoil permeability of the magnet. R_i, R_m, and R_r denote the stator inner radius, the rotor outer radius, and the shaft outer radius, respectively.

As mentioned before, equation (3), the frequency and B_{fe}, are the main factors to the calculation of the stator iron loss. According to equation (2), stator iron loss also depends on stator core volume, which can be calculated by

$$B_g A_g = B_m A_m \tag{10}$$

$$B_m A_m = B_{fe} A_{fe} \tag{11}$$

where A_g and A_m are the air-gap area and the permanent magnet area, respectively.

For the 6s/2p PM motor, the stator tooth width is the same as the stator yoke height [22]. Therefore, the stator tooth width (w_t) and the stator yoke height (h_t) can be calculated by B_g and B_{fe} according to equation (10) and (11)

$$w_t = h_t = \frac{\left(R_i - l_g/2 \right) B_g}{\pi B_{fe}} \tag{12}$$

Then, with a fixed packing factor and the same inner and outer slot areas, the cross-section area of conductors (A_{cond}) can be calculated. Therefore, the electromagnetic torque can be presented as a function of the split ratio (λ) and B_{fe}, and equation (8) can be rewritten by

$$T_{em} = 2 l_a N_s k_w \sqrt{\frac{1}{2 \rho_{cu} N_s}} f(\lambda, B_{fe}) \tag{13}$$

where

$$\begin{aligned} & f(\lambda, B_{fe}) \\ &= \left(\lambda D_o - l_g \right) B_g(\lambda) \sqrt{\frac{A_{cond}(\lambda, B_{fe})}{l_a + l_e(\lambda, B_{fe})}} \sqrt{P_{limit} - P_{fe}(\lambda, B_{fe})} \end{aligned} \tag{14}$$

For a given B_{fe}, the optimal SR for the maximum average torque can be obtained by

$$\frac{\partial f(\lambda)}{\partial(\lambda)} = 0 \tag{15}$$

Fig. 3 depicts the effects of SR and B_{fe} on the average torque. It can be observed that for each B_{fe}, the torque increases at first and then drops with the grow of SR. The same trend can be observed for the relationship between the maximum average torque and B_{fe}. Therefore, with an optimal combination of SR and B_{fe}, the maximum average torque can be achieved. Fig. 4 shows the variations of FE and analytically predicted average torques with SR under the optimal B_{fe} (1.2T). The results predicted by FE and analytical methods have a good agreement in optimal SR and only a slight difference exhibited in the average torque.

As mentioned before, the stator iron loss is considerably large due to high frequency, and thus the effect of the considered stator iron loss on the optimal SR is analyzed in this

section. Fig. 5 depicts the effect on average torque with SR by considering and neglecting stator iron loss. It is clear that compared with considering copper loss only, the considered stator iron loss decreases not only the optimal SR but also the maximum average torque. With the fixed stator loss, the considered stator iron loss leads to the reduced copper loss, thus the reduced electric loading and maximum average torque. In addition, the influence of stator iron loss on the optimal SR can also be verified by FE method, Fig. 14, and the analytical and FE predicted torques have a good agreement. Table II shows the optimized design of the 6s/2p TWHSPM motor.

TABLE II
OPTIMIZED PARAMETERS OF MOTOR WITH TOROIDAL WINDINGS

Optimal split ratio	0.3	Inner tooth width (mm)	5.4
Maximum iron flux density (T)	1.2	Inner tooth height (mm)	10
Stator inner radius (mm)	8.1	Stator yoke height (mm)	5.4
Magnet thickness (mm)	4.05	Slot ratio	0.5

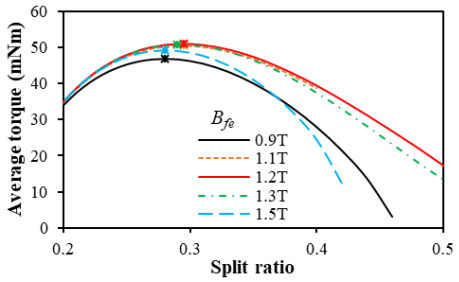

Fig. 3. Relationship between average torque and SR with different B_{fe}.

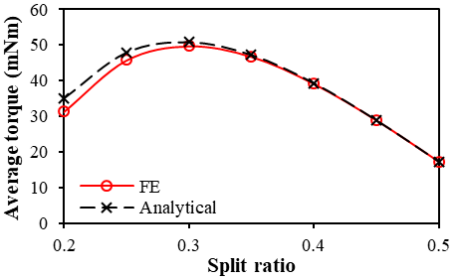

Fig. 4. Variation of FE and analytically predicted average torques with SR (B_{fe}=1.2T).

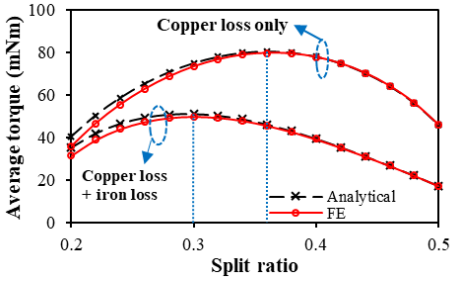

Fig. 5. Variation of average torque with SR by analytical and FE methods (B_{fe}=1.2T).

IV. INFLUENCE OF DESIGN PARAMETERS ON OPTIMAL SPLIT RATIO

A. Influence of Slot Ratio

In section III, the inner and outer slot areas are assumed to be the same. However, the outer slot area usually is designed to be larger than the inner slot area for the forced-air cooling requirement. Thus, the slot ratio (K_a), i.e. the ratio of inner slot to total slot areas, is introduced to determine the influence of the unequal inner and outer slot areas on the optimal SR, Fig. 6. It should be noted that during the variation of the slot ratio, different inner and outer slot areas lead to different packing factors. Since the packing factor in the smaller slot area is larger than that in the larger slot area, the required packing factor is employed in the slot with smaller area and the packing factor in the slot with larger area can subsequently be calculated.

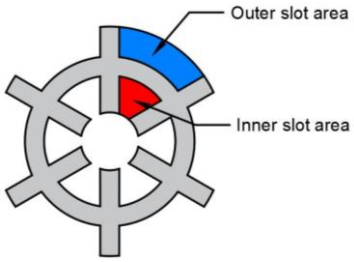

Fig. 6. Inner and outer slot areas of the 6s/2p TWHSPM motor.

Slot ratio should be taken into consideration since it affects the stator iron volume, which will be resulted in the calculation of stator iron loss. Although different slot ratios lead to different end-winding radial lengths, the influence of the copper loss of end-winding radial lengths on the optimal SR is very small considering stator iron loss. Therefore, the torque calculation can be rewritten as

$$T_{em} = 2l_a N_s k_w \sqrt{\frac{1}{2\rho_{cu} N_s}} f(\lambda, B_{fe}) \tag{16}$$

where

$$f(\lambda, B_{fe}) = \left(\lambda D_o - l_g\right) B_g(\lambda) \sqrt{\frac{A_{cond}(\lambda, B_{fe})}{l_a + l_e(\lambda, B_{fe})}} \sqrt{P_{limit} - P_{fe}(\lambda, B_{fe})} \tag{17}$$

and

$$A_{cond} = \begin{cases} A_{s_{in}} k_p \left(K_a \le 0.5\right) \\ A_{s_{out}} k_p \left(K_a > 0.5\right) \end{cases} \tag{18}$$

With the given B_{fe} and K_a, the optimal SR can be obtained by

$$\frac{\partial f(\lambda)}{\partial(\lambda)} = 0 \tag{19}$$

It is assumed that the B_{fe} is fixed as 1.2T, which is the optimal value when the slot ratio is 0.5. Fig. 7 shows the variation of average torque with SR under different slot ratios. It can be seen that for each given slot ratio, the average torque increase at first and then drops with the SR grows, which means the optimal SR for maximum torque can be achieved. Fig. 8 depicts the effect of slot ratio on the maximum average torque and optimal SR. It shows that with a fixed B_{fe}, the increased slot ratio decreases the optimal SR linearly and the maximum average torque can be achieved when the slot ratio is 0.5. The results can be explained by the active slot area, as shown in Figs. 9 and 10. The motor with K_a=0.5 has the largest active slot area and thus it has the largest average torque, Fig. 9. For the optimal SR, the differentials of active slot area curves against SR are shown in the Fig. 10. It depicts that the differential values increase when the slot ratio increases, and thus the motor with larger slot ratio obtains smaller optimal SR. It should be noted that the slot ratio also affects the total slot area, which

leads to the different active slot areas between K_a=0.1/0.9, 0.3/0.7, Fig. 11.

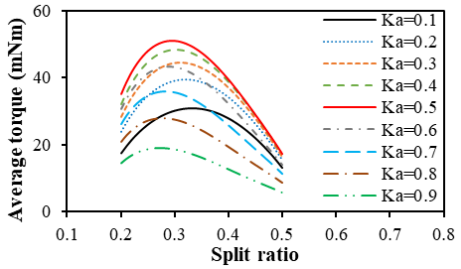

Fig. 7. Relationship between average torque and SR under different slot ratios (B_{fe}=1.2T).

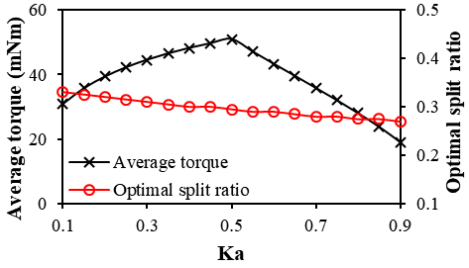

Fig. 8. Relationship between average torque and optimal SR with slot ratio K_a (B_{fe} =1.2T).

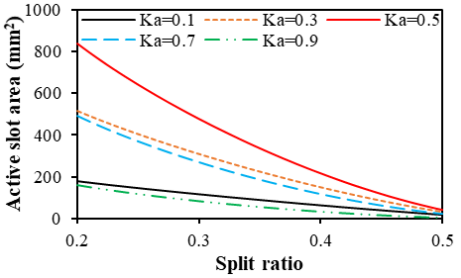

Fig. 9. Influence of SR on active slot area under different slot ratio K_a (B_{fe} =1.2T).

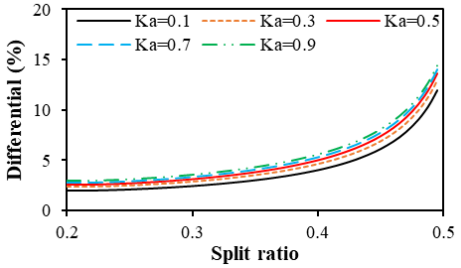

Fig. 10. Variation of differential active slot area curves against SR under different K_a (B_{fe} =1.2T).

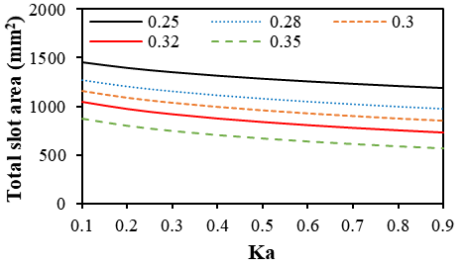

Fig. 11. Variation of total slot area with slot ratio K_a under different SR (B_{fe} =1.2T).

B. *Influence of Maximum Stator Iron Flux Density*

As stated in Section III, the maximum stator iron flux density B_{fe} has important influence on the stator iron loss, which affects the optimal SR with fixed the stator loss. In order to investigate the effect of the B_{fe} on the relationship between optimal SR and slot ratio, different B_{fe} are selected. Figs. 12 and 13 show the variation of average torque with SR under different slot ratios when the B_{fe} is 0.9 T and 1.5T, respectively. It is clear that the maximum average torque can also be achieved when the slot ratio is 0.5. Fig. 14 depicts the influence of B_{fe} and slot ratio on optimal SR. It shows that for any given B_{fe}, the optimal SR drops with the increase of slot ratio. When B_{fe} is larger than 1, the influence of K_a on the optimal SR is significantly large, i.e. large variation range of optimal SR. When B_{fe} is less than 1, the influence of K_a on the optimal SR is relatively small, i.e. small variation range of optimal SR, Fig. 14. Therefore, the optimal SR of the case of B_{fe} larger than 1 is sensitive to the slot ratio, and that of the case of B_{fe} less than 1 is relatively insensitive. Fig. 15 depicts the relationship between maximum average torque and slot ratio under different B_{fe}. It indicates that for any given B_{fe}, the peak value of the maximum torque can be achieved when the slot ratio is 0.5. In addition, the maximum torque difference between different B_{fe} decreases with the increase of slot ratio, when it is larger than 0.5. However, when the slot ratio is smaller than 0.5, the optimal B_{fe} for the maximum torque rises with the decreases of slot ratio. Therefore, considering the design of forced-air cooling channel, i.e. the slot ratio less than 0.5, the relatively large B_{fe} can be selected for enhancing the torque capacity.

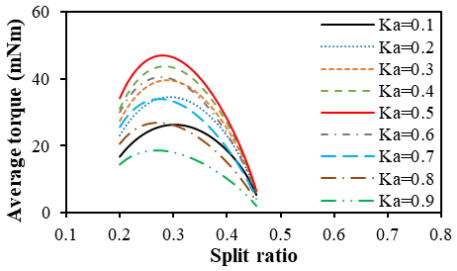

Fig. 12. Relationship between average torque and SR (B_{fe}=0.9T).

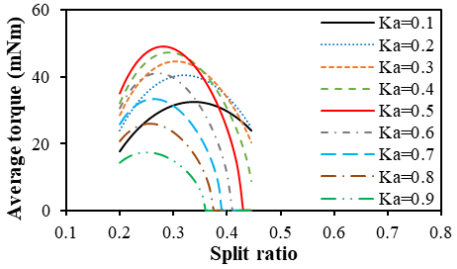

Fig. 13. Relationship between average torque and SR (B_{fe}=1.5T).

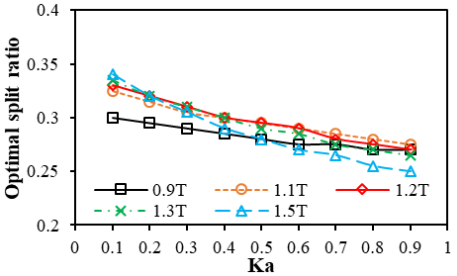

Fig. 14. Influence of K_a on optimal SR under different B_{fe}.

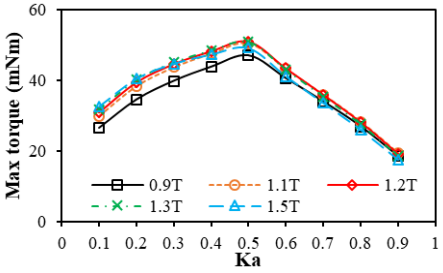

Fig. 15. Relationship between K_a and maximum average torque with different B_{fe}.

C. *Influence of Tooth-tips*

In the foregoing analyses, the motor employs straight tooth without tooth-tips for simplifying manufacturing process. However, the tooth-tips can reduce the leakage flux and increase the phase inductance. Therefore, in this section, the influence of tooth-tips on the maximum torque and optimal SR will be investigated. The cross section of the 6s/2p TWHSPM motor with tooth-tips is illustrated in Fig. 16. The active slot area considering the tooth-tips can be given by

$$A_{S_{in}} = \pi \left[\begin{array}{c} h_{out}^2 + h_t^2 + 2h_{out}h_t - \left(D_s + \frac{N_s w_t}{\pi} \right) h_{out} - (D_s + \frac{N_s w_t}{\pi}) h_t \\ -h_{tt}^2 - 2\pi h_{tt} - \frac{N_s w_t}{\pi} \frac{D_s}{2} (1-\lambda) + \frac{N_s w_t}{\pi} h_{tt} \end{array} \right] \quad (20)$$

where h_{tt} is the tooth-tip height.

Fig. 17 depicts when the slot ratio is 0.5, the effect of SR under different B_{fe} with 1mm tooth-tip thickness on average torque. The analytical and FE-predicted torques with and without tooth-tips have a good agreement, Fig. 18. For a given B_{fe}, tooth-tips have almost no influence on the variations of maximum torque and optimal SR with slot ratio, as shown in Figs.19 and 20. Figs. 21 and 22 show the flux distributions and torque waveforms of TWHSPM motors with different shapes of tooth-tip, such as parallel tooth-tip, round tooth-tip, and tiered tooth-tip. It shows that the shape of tooth-tip has almost no effect on the flux distribution, electromagnetic torque, and torque ripple.

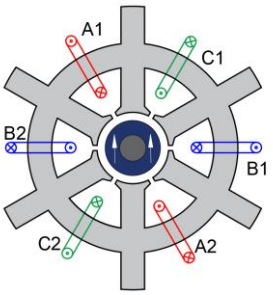

Fig. 16. Cross section of 6s/2p TWHSPM motor with tooth-tips.

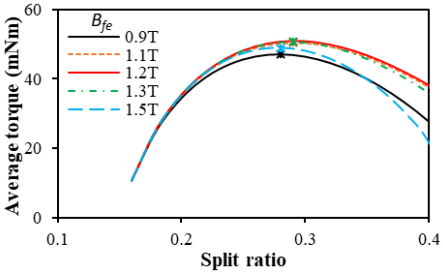

Fig.17. Variation of average torque with SR and B_{fe} with tooth-tip (K_a =0.5, h_{tt}=1mm).

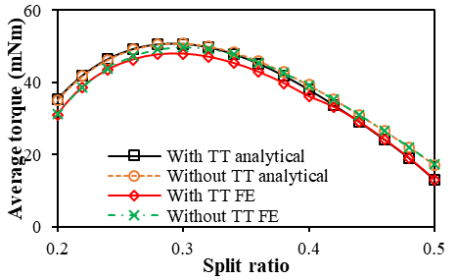

Fig. 18. Variation of FE and analytically predicted average torques with SR (B_{fe}=1.2T).

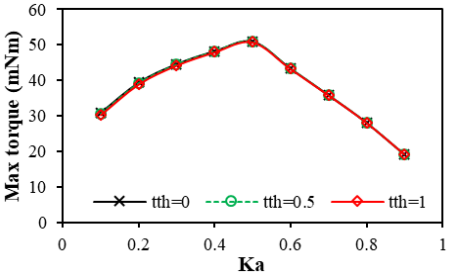

Fig. 19. Influence of K_a and tooth-tip thickness on maximum average torque (B_{fe} =1.2T).

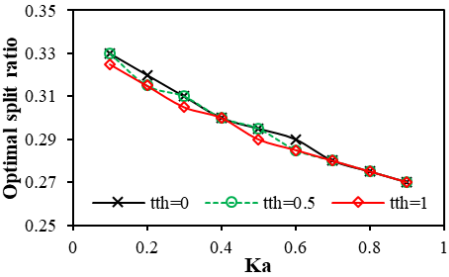

Fig. 20. Influence of K_a and tooth-tip thickness optimal SR (B_{fe} =1.2T).

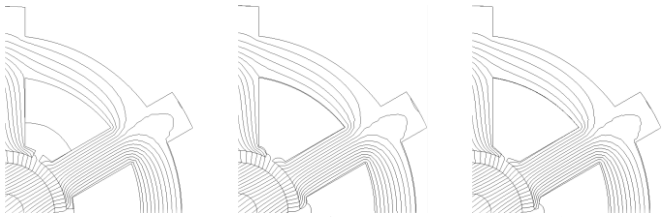

Fig. 21. Flux distributions of TWHSPM motors with different shapes of tooth-tip. (a) Parallel tooth-tip. (b) Round tooth-tip. (c) Tiered tooth-tip.

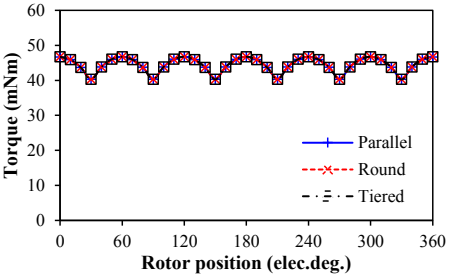

Fig. 22. Torque waveforms of TWHSPM motors with different shapes of tooth-tip.

In summary, with the increase of slot ratio, the optimal SR decreases linearly and the maximum torque increases firstly and then decreases. With the increase of B_{fe}, the optimal SR becomes more sensitive to the slot ratio. When the slot ratio is less than 0.5, the relatively large B_{fe} is better for torque enhancement. In addition, the tooth-tip has almost no influence

on the relationship among optimal SR, maximum torque, slot ratio, and B_{fe}.

V. Experimental Validation

In this section, some of predicted results are verified by the measured results of 6s/2p TWHSPM prototype motor with 0.5 slot ratio. Fig. 23 indicates the stator structure of the prototype motor, the shaft-bearing-blade system, the forced-air cooling system, and the house structure.

Table III provides the value of phase resistance and winding inductance of the prototype, which are measured by a LCR meter. Due to manual winding, the extra end-winding length (l_{ex}) is set to be 1.5mm, the analytically predicted resistance has good agreement with the measured result (1Hz). It should be noticed that the measured resistance under high frequency (1833Hz) is substantial larger than that under low frequency (1Hz), this means the AC copper loss of toroidal windings is large under high frequency. However, it can be avoided by Litz-wire and is ignored in the previous analysis. In table III, since the 2D-FE model provide an ideal winding inductance which neglecting end-winding inductance, the FE predicted value is smaller than the measured winding inductance. Due to skin effect, the measured inductance drops when the frequency increases.

Fig. 24 shows the analytically predicted, FE computed, and measured back-EMFs of phase A in the prototype motor at 11 krpm. It can be seen that the FE predicted and measured results have a good agreement but the analytical prediction is slightly larger due to neglecting the flux leakage caused by straight tooth without tooth-tips. The static torque is measured by a test rig in this paper since it is difficult to measure the torque under high speed operation in general [28], Fig. 25. The test results show that the measured open-circuit static torque, i.e. cogging torque, is almost zero, which is the same as the predicted result. The measured on-load static torque has a good agreement with the FE predicted result, Fig. 26. With the phase current rises, the maximum static torque increases linearly, and the measured maximum static torques have a great agreement with the FE calculations, Fig. 27. The measured phase current and terminal voltage waveforms of the prototype motor at 110 krpm are shown in Fig. 28. In addition, Fig. 29 shows the prototype motor operates at 120 krpm which above the rated speed.

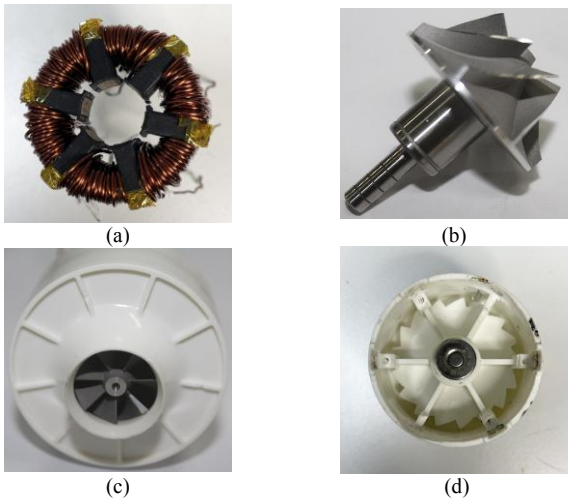

Fig. 23. Prototype of the 6s/2p TWHSPM motor. (a) Stator. (b) Shaft-bearing-blade system. (c) Forced air cooling system. (d) House.

TABLE III
Predicted and Measured Winding Resistances and Inductances

Resistance (mΩ)			Inductance (μH)		
Predicted	Measured (1Hz)	Measured (1.83 kHz)	Predicted	Measured (1Hz)	Measured (1.83kHz)
40.05	44.16	72.80	19.5	26.32	23.16

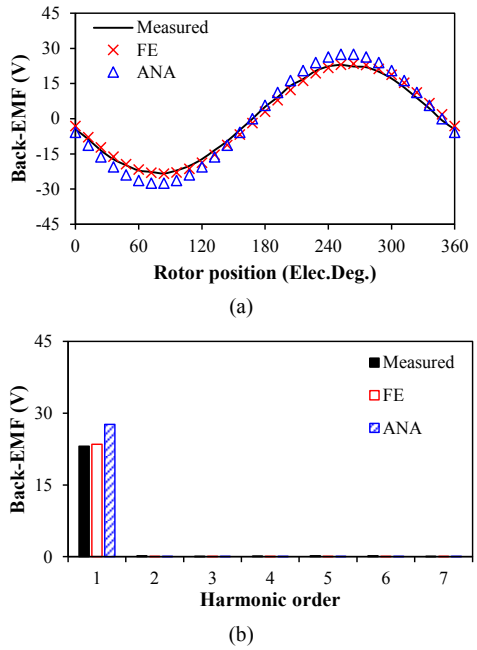

Fig. 24. Back-EMF of phase A of FE calculated, analytical predicted, and measured in the 6s/2p TWHSPM motor at 110 krpm. (a) Waveforms. (b) Spectra.

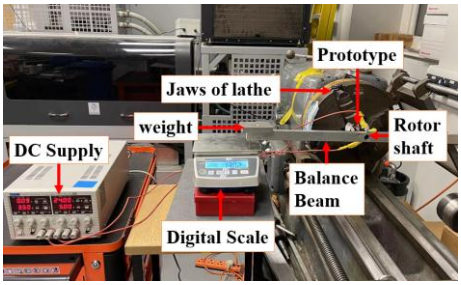

Fig. 25. Static torque measurement test rig.

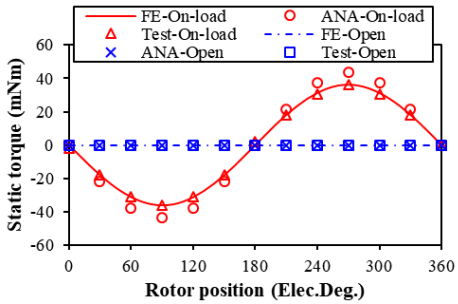

Fig. 26. Measurement and FE predicted open-circuit and on-load static torques under the phase currents of $I_A = -I_B = 5$ A, I_C=0A.

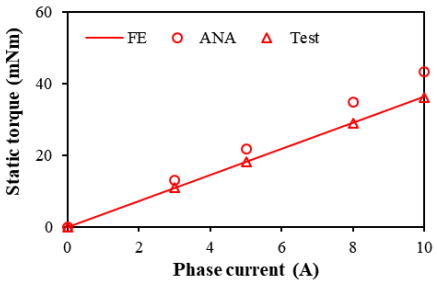

Fig. 27. Maximum measurement and FE predicted static torques with various phase currents.

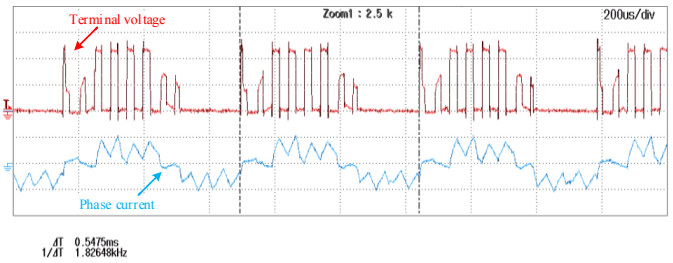

Fig. 28. Measured phase current and terminal voltage waveforms of the 6s/2p TWHSPM motor at 110 krpm, i.e. f=1.83 kHz, with speed control (10.0V/div; 20.0A/div; U_{dc} =25.2V).

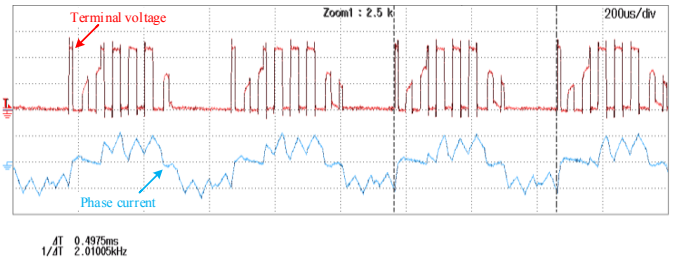

Fig. 29. Measured phase current and terminal voltage waveforms of the 6s/2p TWHSPM motor at 120 krpm, i.e. f=2.00 kHz, with speed control (10.0V/div; 20.0A/div; U_{dc} =25.2V).

VI. Conclusion

In this paper, the optimal split ratio of the 6s/2p TWHSPM motor has been investigated by analytical method considering stator copper loss and iron loss, and validated by FE method. Meanwhile, the influences of slot ratio, B_{fe}, and tooth-tips on optimal SR are investigated. It depicts that the maximum torque can be achieved when inner slot areas equal to outer slot area, i.e. slot ratio is 0.5. When the slot ratio increases, the optimal SR decreases, and the results are affected by B_{fe}. Some of the analytical predictions have been validated by FE method and experiments.

References

[1] N. Bianchi, S. Bolognani, and F. Luise, "Analysis and design of a PM brushless motor for high-speed operations," *IEEE Trans. Energy Convers.*, vol. 20, no. 3, pp. 629-637, Sept. 2005.

[2] D. Gerada, A. Mebarki, N. L. Brown, C. Gerada, A. Cavagnino, and A. Boglietti, "High-Speed electrical machines: technologies, trends, and developments," *IEEE Trans. Ind. Electron.*, vol. 61, no. 6, pp. 2946-2959, Jun. 2014.

[3] A. Tenconi, S. Vaschetto, and A. Vigliani, "Electrical machines for high-speed applications: design considerations and tradeoffs," *IEEE Trans. Ind. Electron.*, vol. 61, no. 6, pp.3022-3029, Jun. 2014.

[4] J. X. Shen, X. Qin, and Y. Wang, "High-speed permanent magnet electrical machines — applications, key issues and challenges," *CES Transactions on Electrical Machines and Systems*, vol. 2, no. 1, pp. 23-33, Mar. 2018.

[5] G. Du, N. Huang, H. He, G. Lei, and J. Zhu, "Parameter design for a high-speed permanent magnet machine under multiphysics constraints," *IEEE Trans. Energy Convers*, vol. 35, no. 4, pp. 2025-2035, Dec. 2020.

[6] X. Jannot, J. Vannier, C. Marchand, M. Gabsi, J. Saint-Michel and D. Sadarnac, "Multiphysic modeling of a high-speed interior permanent-magnet synchronous machine for a multiobjective optimal design," *IEEE Trans. Energy Convers*, vol. 26, no. 2, pp. 457-467, June 2011.

[7] Z. Kolondzovski, A. Arkkio, J. Larjola and P. Sallinen, "Power limits of high-speed permanent-magnet electrical machines for compressor applications," *IEEE Trans. Energy Convers*, vol. 26, no. 1, pp. 73-82, March 2011.

[8] F. R. Ismagilov, N. Uzhegov, V. E. Vavilov, V. I. Bekuzin and V. V. Ayguzina, "Multidisciplinary design of ultra-high-speed electrical machines," *IEEE Trans. Energy Convers*, vol. 33, no. 3, pp. 1203-1212, Sept. 2018.

[9] Z. Q. Zhu, K. Ng, and D. Howe, "Design and analysis of high-speed brushless permanent magnet motors," *International Conference on Electrical Machines and Drives (Conf. Publ. No. 444)*, Cambridge, UK, 1997, pp. 381-385.

[10] D. E. Hesmondhalgh, D. Tipping, and M. Amrani, "Design and construction of a high-speed high performance direct-drive handpiece," *IEE Proc. B – Elec. Power Appl.*, vol. 134, no. 6, pp. 286-296, Nov. 1987.

[11] K. Shigematsu, J. Oyama, T. Higuchi, T. Abe, and Y. Ueno, "The study of eddy current in rotor and circuit coupling analysis for small size and ultra-high speed motor," *International Power Electronics and Motion Control Conference* (*IPEMC*), Xi'an, China, 2004, pp. 275-279, vol.1.

[12] T. Noguchi, Y. Takata, Y. Yamashita, Y. Komatsu, and S. Ibaraki, "220000 r/min 2kW PM motor drive for turocharger," *IEEJ Trans. Ind. Appl.*, vol. 125, no. 9, pp. 854–861, Sep. 2005.

[13] T. R. He, Z. Q. Zhu, F. Xu, H. Bin, D. Wu, L. M. Gong, and J. T. Chen, "Comparative study of 6-slot/2-pole high-speed permanent magnet motors with different winding configurations," *IEEE Trans. Ind. Appl.*, vol. 57, no. 6, pp. 5864-5875, Nov.-Dec. 2021.

[14] T. He, Z. Q. Zhu, F. Xu, Y. Wang, B. Hong and L. Gong, "Electromagnetic performance analysis of 6-Slot/2-Pole high-speed permanent magnet motors with coil-pitch of two slot-pitches," *IEEE Trans. Energy Convers. Early access.*

[15] F. X. Wang, M. Zong, W. P. Zheng, and E. L. Guan, "Design features of high speed PM machines," *International Conference on Electrical Machines and Systems (ICEMS),* Beijing, China, 2003, pp. 66-70, vol. 1.

[16] C. Zwyssig, J. W. Kolar, W. Thaler, and M. Vohrer, "Design of a 100W, 500000 rpm permanent-magnet generator for mesoscale gas turbines," *Conf. Rec. IEEE IAS Annu. Meeting*, Sep. 2005, pp. 253–260.

[17] A. Borisavljevic, S. Jumayev, and E. Lomonova, "Toroidally-wound permanent magnet machines in high-speed applications," *International Conference on Electrical Machines (ICEM)*, Berlin, Germany, 2014, pp. 2588-2593.

[18] F. Xu, T. R. He, Z. Q. Zhu, Y. Wang, H. Bin, D. Wu, L. M. Gong, and J. T. Chen, "Influence of slot number on electromagnetic performance of 2-pole high-speed permanent magnet motors with toroidal windings," *IEEE Trans. Ind. Appl.*, vol. 57, no. 6, pp. 6023-6033, Nov.-Dec. 2021.

[19] F. B. Chaaban, "Determination of the optimum rotor/stator diameter ratio of permanent magnet machines," *Electr. Mach. Power Syst.*, 1994, 22, pp. 521–531.

[20] F. B. Chaaban and A. El-Hajj, "A cost-effective design approach for permanent magnet brushless machines," *Electr. Mach. Power Syst.*, 2000, 28, pp. 893–900.

[21] J. D. Ede, Z. Q. Zhu, and D. Howe, "Optimal split ratio for high-speed permanent magnet brushless DC motors," *International Conference on Electrical Machines and Systems (IEEE Cat. No.01EX501)*, Shenyang, China, 2001, pp. 909-912, vol.2.

[22] Y. Pang, Z. Q. Zhu, and D. Howe, "Analytical determination of optimal split ratio for permanent magnet brushless motors," *IEE Proceedings Electric Power Appl.*, vol. 153, no. 1, pp. 7-13, 2006.

[23] Y. Wang, S. Guo, Y. Li, Z. Chen, Y. Wang, and Z. Zhu, "Investigation of optimal split ratio for high-speed permanent magnet brushless machines," *IEEE Trans. Magnetics*, vol.54, no.11, Article No: 8105605, 2018.

[24] J. Ma and Z. Q. Zhu, "Optimal split ratio in small high speed PM

machines considering both stator and rotor loss limitations," *CES Transactions on Electrical Machines and Systems*, vol. 3, no. 1, pp. 3-11, Mar. 2019.

[25] T. Reichert, T. Nussbaumer, and J. W. Kolar, "Split ratio optimization for high-torque PM motors considering global and local thermal limitations," *IEEE Trans. Energy Convers.*, vol. 28, no. 3, pp. 493-501, Sept. 2013.

[26] G. Bertotti, "General properties of power losses in soft ferromagnetic materials," *IEEE Trans. Magn.*, vol. 24, no. 1, pp. 621-630, Jan. 1988.

[27] N. Bianchi, S. Bolognani, and F. Luise, "Potentials and limits of high-speed PM motors," *IEEE Trans. Ind. Appl.*, vol. 40, no. 6, pp. 1570-1578, Nov.-Dec. 2004.

[28] Z. Q. Zhu, "A simple method for measuring cogging torque in permanent magnet machines," *IEEE Power Energy Soc. General Meeting, Calgary*, AB, Canada, 2009, pp. 1–4.

F. Xu received the B.Eng. and M.Sc. degrees in electrical engineering from Nanjing Forestry University, Nanjing, China, in 2015 and The University of Sheffield, Sheffield, U.K. in 2016, respectively. She is currently working toward the Ph.D. degree in electrical engineering at the Department of Electronic and Electrical Engineering, The University of Sheffield, Sheffield, U.K. Her major research interests include design and analysis of permanent magnet brushless motors for high-speed application.

T. R. He received the B.Eng. and M.Sc. degrees from Harbin Institute of Technology, Harbin, China, in 2014, and The University of Sheffield, Sheffield, U.K. in 2017, respectively, and the Ph.D. degree from the University of Sheffield, Sheffield, U.K., in 2021, all in electrical engineering. From 2014 to 2016, he was an Engineer with Shanghai Electric Wind Power Group Co., Ltd., Shanghai, China. He is currently an assistant professor with the School of Electronic and Information Engineering, Tongji University, Shanghai, China. His major research interests include design and analysis of high-speed permanent magnet brushless motors and permanent magnet synchronous motors.

Z. Q. Zhu received the B.Eng. and M.Sc. degrees from Zhejiang University, Hangzhou, China, in 1982 and 1984, respectively, and the Ph.D. degree from The University of Sheffield, Sheffield, U.K., in 1991, all in electrical and electronic engineering. Since 1988, he has been with The University of Sheffield, where he is currently a Professor with the Department of Electronic and Electrical Engineering, the Head of the Electrical Machines and Drives Research Group, the Royal Academy of Engineering/Siemens Research Chair, the Academic Director of Sheffield Siemens Gamesa Renewable Energy Research Centre, the Director of Midea Electrical Machines and Control Systems Research Centres, and the Director of Sheffield CRRC Electric Drives Technology Research Centre. His current major research interests include design and control of permanent magnet brushless machines and drives for applications ranging from electrified transportation through domestic appliance to renewable energy. He is the recipient of 2019 IEEE Industry Applications Society Outstanding Achievement Award and the 2021 IEEE Nikola Tesla Award. He is a Fellow of the Royal Academy of Engineering, a Fellow of IEEE, and a Fellow of the IET.

H. Bin received the B.Eng. and M.Sc. degrees in electrical engineering from Tongji University, Shanghai, China, in 2002 and 2015, respectively. He is currently working at the Midea Group Corporate Research Center, Shanghai, China. His current research interests include high speed BLDC motor drives and PWM converters.

D. Wu received the M.Sc. degree in electrical engineering from the Huazhong University of Science and Technology, Wuhan, China, in 2011, and the Ph.D. degree in electronic and electrical engineering from the University of Sheffield, Sheffield, U.K., in 2015. Since 2011, he has been working with the Midea Welling Motor Technology (Shanghai) Co., Ltd., Shanghai, China, and is currently Head of Motor Development Department, Welling, Midea Group. His major research interests include design and analysis of permanent-magnet brushless machines.

L. M. Gong received the B.Eng. and M.Sc. degrees in electrical engineering from Huazhong University of Science and Technology, Wuhan, China, in 2001 and 2004, respectively, and the Ph.D. degree in electrical and electronic engineering from the University of Sheffield, Sheffield, U.K., in 2012. From 2004 to 2008, he was with Emerson Network Power Company Ltd., Shenzhen, China, as a Research Engineer working to develop general purpose ac drives. Since 2012, he has been with the Midea Welling Motor Technology (Shanghai) Co., Ltd. His research interests include control of permanent-magnet brushless machines and power electronics.

J. T. Chen received the B.Eng. and M.Sc. degrees from Huazhong University of Science and Technology, Wuhan, China, in 2001 and 2004, respectively, and the Ph.D. degree from The University of Sheffield, Sheffield, U.K., in 2009, all in electrical engineering. From 2004 to 2006, he was an Engineer with Delta Electronics (Shanghai) Company, Ltd., Shanghai, China. He is currently a General Manager of Midea Automotive Components Ltd and with the Midea Shanghai Motors and Drives Research Center, Shanghai, China. His major research interests include design of permanent magnet machines.